Modeling a Nozzle in a Borehole

E. Holzbecher, F. Sun
Georg-August Universität Göttingen
*Goldschmidtstr. 3, 37077 Göttingen, GERMANY; E-mail: eholzbe@gwdg.de

Abstract: A nozzle, installed in an injecting borehole, can enhance the infiltration rate into the subsurface porous medium significantly. Using Finite-Element simulations of turbulent flow we examine the effect of the nozzle and screen geometry on the flow field within the borehole. This is a first step towards a model in which free flow in the borehole will be coupled with porous media flow in the surrounding.

Keywords: Nozzle, borehole, injection, CFD, turbulent flow

1. Introduction

Within a borehole a nozzle can be installed in order to increase the efficiency of fluid injection. The new technology is currently explored within the DSI research project, funded by DBU, in Germany. DSI stands for German 'Düsensauginfiltration', which letterly means nozzle suction infiltration (Holzbecher *et al.* 2011, Jin *et al.* 2011). The position of the nozzle is located near the perforated casing of the injection well. Several types of nozzles are used in practical applications. Figure 1 depicts a nozzle and the slotted filter screen (DSI nozzle and Klaas filter). The slots are the outlets to the borehole and the adjacent porous medium, which is not part of the model region up to now.
The local fluid velocity at and near the nozzle outlet in increased. In addition, the shape of the nozzle and the boundaries of casing and borehole also play a role for the injection. Different modeling methods, settings of meshes, nozzle geometries and variations of outlet flux through perforated casing are discussed in the following, using modelling with COMSOL Mutiphysics 4.4.

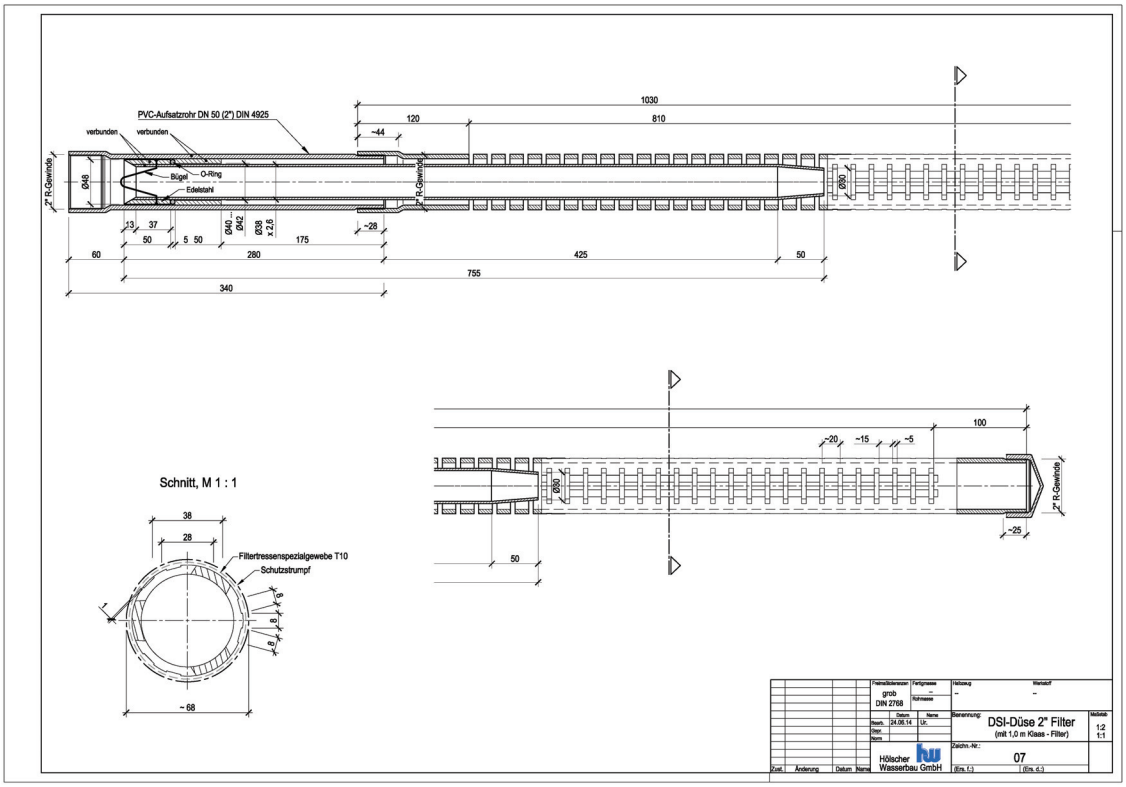

Figure 1: Nozzle and filter screen blueprint

Yu *et al.* (2012) dicuss geometry options concerning turbulent flow within a nozzle; the Reynolds-numer is around 50.000. They examine modified geometries (extended, grooved, ringed) and use different models for turbulent closure (Spalart-Allmaras, k-ε, k-ω and Reynolds stress model). Up to now there are no studies on the turbulent flow build-up in a vertical pipe due to a nozzle.

2. Model Set-up

A model is set up for a typical nozzle design as applied in practice. Figure 2 shows a 2D model region in the axi-symmetric coordinate system, here for a slightly simplified nozzle/casing geometry. Flow is downward through the nozzle, with decreased cross-section. In the model the fluid leaves through nine slots in the perforated screen. Reference flow velocity is 30 m^3/h.
The filter screen in real applications has 3D features, which are neglected here for the first approach. In reality the cross-section through the filter shows three horizontal separated slots, as shown in the lower left part of Figure 1.
Another simplification is that we model steady-states only and neglect the surely transient nature of turbulence (Wilcox 2006). In the physical formulation of turbulence the real fluctuating nature of the velocity vectors can mostly not be considered in detail. Differential equations are formulated for mean variables, velocities and pressure. Fluctuations from the mean, spatially and temporally, are not considered in detail, but lumped in energy and dissipation terms, which are used for the closure of the model (Wilcox 2006).
The model is based on the Navier-Stokes equations. Turbulence closures are the standard two-equation k-ε and k-ω approaches, with turbulent kinetic energy k, turbulent dissipation rate ε and turbulent dissipation rate ω. We use constraints and boundary conditions, and wall functions close to walls. At outlets we specify pressure as Dirichlet conditions. In order to obtain appropriate distributions of k, ε, and ω at the inlet (top of Figure 2) a pipe model (not shown in Figure 2) is computed in a pre-run before the nozzle model. The result of the pipe model at the outlet is then taken as inlet boundary condition for the nozzle.

By changing modeling methods, fluid rates, setting of mesh and boundary layers, we first explored several different numerical settings. First studies were performed for a hypothetical simpler nozzle designs in order to explore numerical approaches and meshing features. Particularly k-ω and k-ε closures for turbulence were compared.

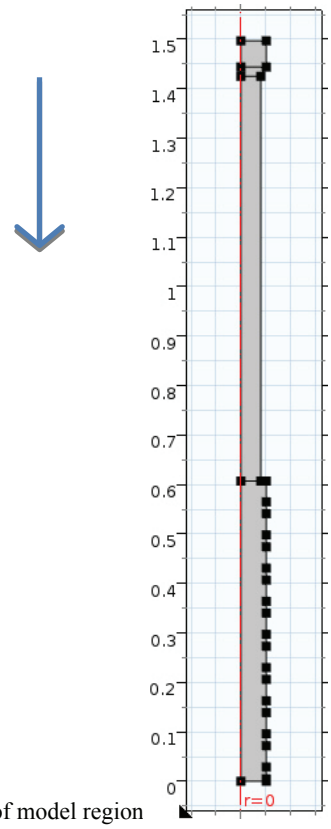

Figure 2: Sketch of model region

3. Results

Figure 3 presents the wall lift-off in viscous units of turbulent flow modeled by k-ω and k-ε approaches in the simplified nozzle model (without perforated screen) for a sufficiently refined mesh.
We used free triangular meshing, except from the boundary layer, where quadrilateral elements are applied. At the outer boundary we used mesh and corner refinement for the solid walls. Moreover we used a resolution of six layers for the boundary layer with a streching factor of 1.2. The thickness of the first layer is determined automatically. The wall-lift off in viscous units is defined by:

$$\delta_w^+ = \rho u_\tau \delta_w / \mu \qquad (1)$$

with fluid density ρ and viscosity μ. u_τ is the friction velocity, given by $u_\tau = C_\mu^{1/4}\sqrt{k}$ with the empirical constant $C_\mu = 0.09$. δ_w corresponds with the distance from the wall, where the logarithmic layer meets the viscous sub-layer. The latter is usually not resolved in models (Kuzmin *et al*. 2007). If the mesh is too coarse, δ_w^+ exceeds the recommended value of 11.06 (see also: Djojodihardjo & Abdul Hamid 2012), which can here be observed for the *k*-ε closure. Clearly the *k*-ω model delivers the required wall-lift off in viscous units along the solid walls of 11.06 (COMSOL Multiphysics, CFD Module 2013), while the *k*-ε model still shows significant deviations. Therefore we recommend the *k*-ω approach for such simulations and used it ourselves for further modeling for the real nozzle design.

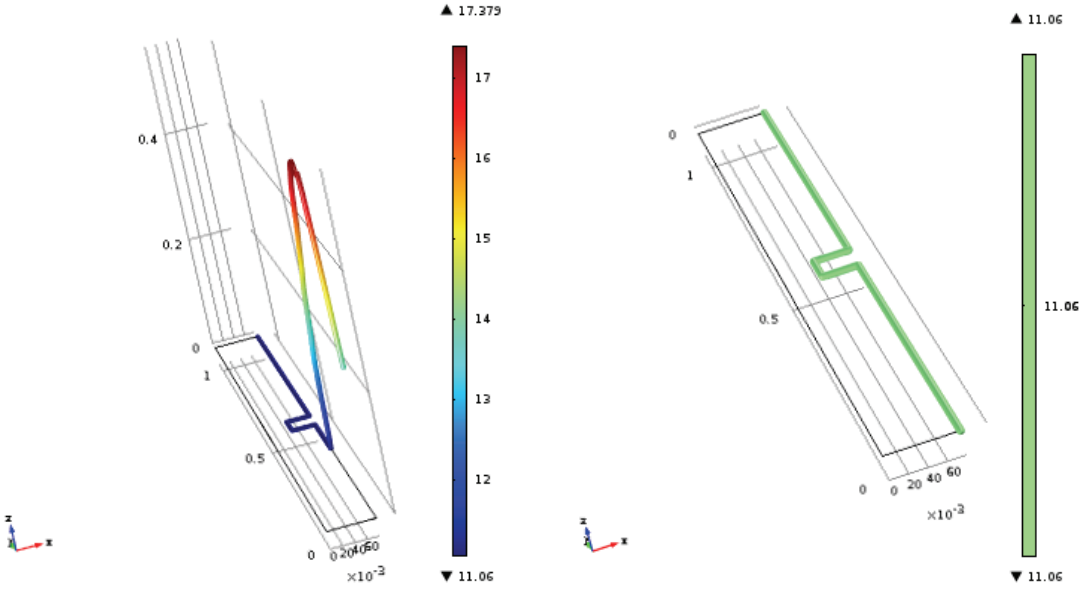

Figure 3: Wall lift-off, depending on turbulent closure; left: *k*-ε, right: *k*-ω

The mesh settings from the simplified nozzle geometry were adopted in the model of the DSI-nozzle including the performated screen. We examined pressure, mean velocity, recirculation length and wall lift-off for various settings of mesh and boundary layer properties. Figure 4 shows the velocity size at the outlet of the nozzle and below. Clearly a flow phenomenon as a fast jet with increased flow velocity develops within the nozzle. In the center high velocities remain for a long part after passing the outlet and only gradually decrease, when the lower closed boundary is approached. In the 3D visualisation the lowest slot is clearly visible, due to increased velocities, while the other slots are hardly to see. However, even in the lowest slot with obviously highest flow the velocities are smaller than in the jet.

Figure 5 shows the flow field visualized by velocity size and streamlines. A constant pattern of vertical turbulent flow developes within the entry pipe and changes only after the cross-section narrows within the nozzle. A jet of increased velocity leaves the nozzle and speed only diminishes, when the closed bottom cap is approached. A small eddy can be observed in the 'blind' edge behind the nozzle and a even smaller one at the very bottom.

The outflow is unevenly distributed between the slots. Outlet flux entirely occurs through the three outlet boundaries near the bottom of the pipe. The share of outgoing flux through for each outlet (from bottom to top) is shown in Figure 6. The lowermost slot releases more than 70% of the flux, the second lowest slot about 20%. All other slots together count up to less than 10%.

We examined if that relation changed with the flow rate through the nozzle. It was found that the contribution of each slot outlet boundary does not change when flow rate changes from 7.5 m^3/h to 90 m^3/h. Figure 6 also depicts these findings. We suggest that values below zero for some outflow slots are probably due to numerical inaccuracies and do not represent inflow.

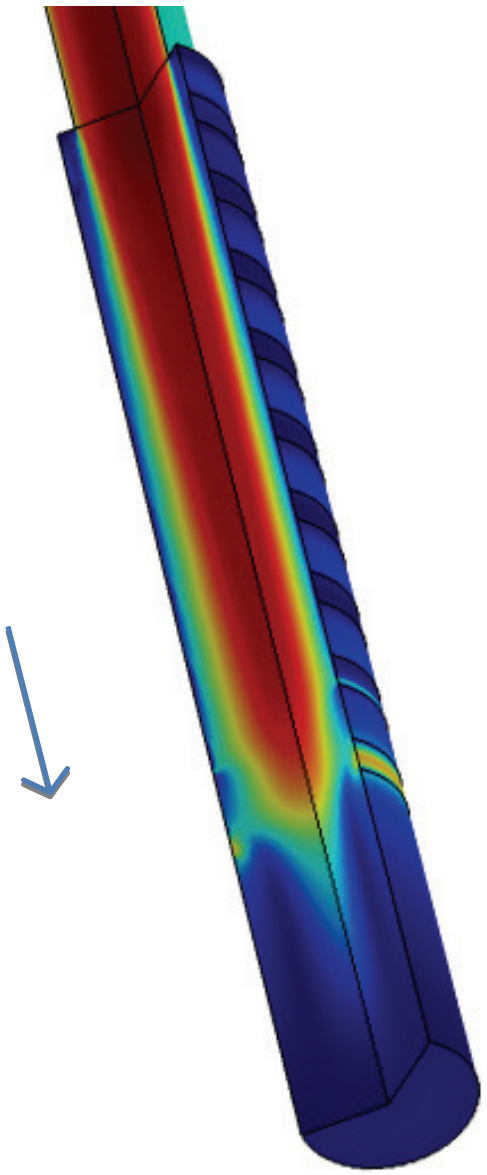

Figure 4: 3D view of flow between nozzle and casing, represented by velocity size (red = high, blue=low)

4. Conclusion and Discussion

By using COMSOL Multiphysics 4.4, the turbulent flow modeled by *k*- ω and *k*- ε methods through different meshed borehole nozzle have been analyzed by comparing pressure, mean velocity, recirculation length and etc.. The results demonstrate that *k*- ω method is much better than *k*- ε method. Meshing, especially concerning the boundary layers, plays a major role to obtain a high accuracy of the results.

Futhermore, the outlet boudaries at the bottom play a dominant role concerning outflow and thus a most relevant for an effective injection. The Dirichlet condition for hydraulic pressure is probably inappropriate for the conditions at the perforation of the borehole, where free flow is changing to porous media flow.

In a next step we intend to extend the model to include the borehole and the porous medium adjacent to the borehole. In the extended model we have to consider the transition from free fluid to porous media flow, but also from turbulent to laminar conditions. In the surrounding of the borehole turbulent flow will endure locally around the perforations, only.

Modelling of such combined regimes is best performed using the Brinkman model, in which both viscous damping, as appearing in free fluids, and resistence from a porous medium can be considered (Holzbecher *et al*. 2007, Holzbecher *et al*. 2010).

The results are of high importance for the practice of water injection into aquifers. As the lower slots are unequally more relevant for the hydraulics of the entire installation, their position should be oriented on the more permeable layers within the porous medium, the so-called DSI-layers.

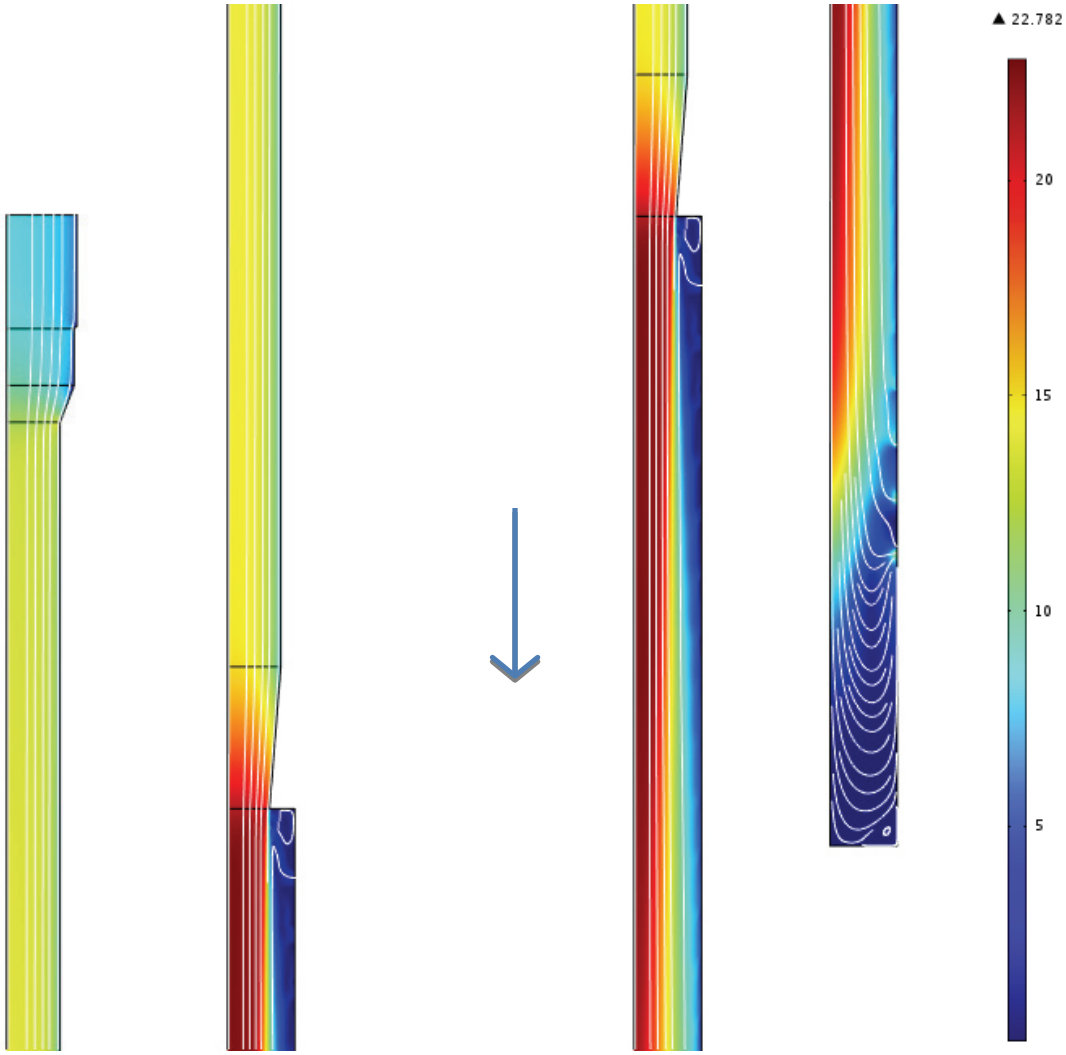

Figure 5: Velocity size (color, [m/s]) and streamlines within the nozzle and casing

References

1. COMSOL Multiphysics, CFD-Module, User's Guide, Version 4.4 (2013)
2. Djojodihardjo H., Abdul Hamid M.F., Computational study on the influence of Coanda jet on airfoils: two-dimensional case, 28th Intern. Congress Aeronaut. Sci. (2012)
3. Holzbecher E., Jin Y., Ebneth S., Borehole pump & inject: an environmentally sound new method for groundwater lowering, International Journal of Environmental Protection, **1**(4), 53-58 (2011)
4. Holzbecher E., Krumbholz S., Modelling of channel - gas diffusion layer systems, COMSOL Conf., Grenoble, Proceedings, 392-397 (2007)
5. Holzbecher E., L. Wong, M. Litz, Modelling flow through fractures in porous media, COMSOL Conf., Paris (2010)
6. Jin Y., Holzbecher E., Oberdorfer P., Simulation of a novel groundwater lowering technique using arbitrary Lagrangian-Eulerian method, COMSOL Conf., Stuttgart (2011)
7. Kuzmin, D., Mierka, O., Turek, S., On the implementation of the k-ε turbulence model in incompressible flow solvers based on a Finite Element discretization, Int. Journal of Computing Science and Mathematics, **1**(2–4), 193–206 (2007)
8. Wilcox, D.C., *Turbulence Modeling for CFD*, 3rd Edition, DCW Industries (2006)

9. Yu Y., Shademan M., Barron R.M., Balanchandar R., CFD study of effects of geometry variations on flow in a nozzle, Eng. Appl. of Comp. Fluid Mech., **6**(3), 412-425 (2012)

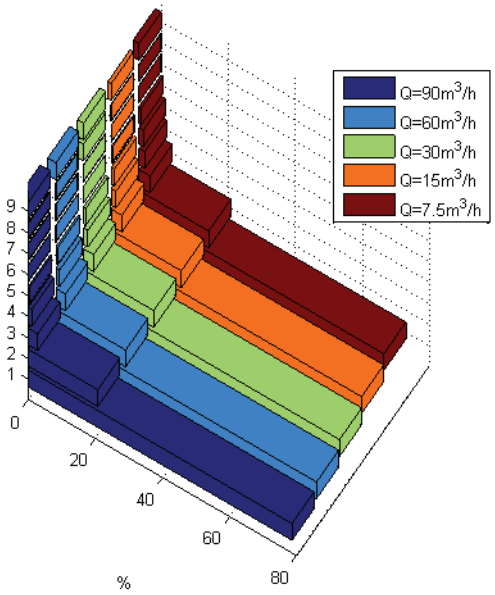

Figure 6: Contribution of outlets to total outflow (%); 1 is lowest, 9 is uppermost outlet

Acknowledgement

The authors appreciate the support of 'Deutsche Bundesstiftung Umwelt (DBU)' for funding within the DSI project (AZ28299-23).